nature chemical biology

ARTICLE

PUBLISHED ONLINE: 28 AUGUST 2011 | DOI: 10.1038/NCHEMBIO.640

TRPA1 underlies a sensing mechanism for O_2

Nobuaki Takahashi[1–3], Tomoyuki Kuwaki[4], Shigeki Kiyonaka[1,2,5], Tomohiro Numata[1,2], Daisuke Kozai[1,2], Yusuke Mizuno[1,2], Shinichiro Yamamoto[1,2], Shinji Naito[6], Ellen Knevels[7,8], Peter Carmeliet[7,8], Toru Oga[9], Shuji Kaneko[10], Seiji Suga[1], Toshiki Nokami[1], Jun-ichi Yoshida[1] & Yasuo Mori[1,2,5]*

Oxygen (O_2) is a prerequisite for cellular respiration in aerobic organisms but also elicits toxicity. To understand how animals cope with the ambivalent physiological nature of O_2, it is critical to elucidate the molecular mechanisms responsible for O_2 sensing. Here our systematic evaluation of transient receptor potential (TRP) cation channels using reactive disulfides with different redox potentials reveals the capability of TRPA1 to sense O_2. O_2 sensing is based upon disparate processes: whereas prolyl hydroxylases (PHDs) exert O_2-dependent inhibition on TRPA1 activity in normoxia, direct O_2 action overrides the inhibition via the prominent sensitivity of TRPA1 to cysteine-mediated oxidation in hyperoxia. Unexpectedly, TRPA1 is activated through relief from the same PHD-mediated inhibition in hypoxia. In mice, disruption of the *Trpa1* gene abolishes hyperoxia- and hypoxia-induced cationic currents in vagal and sensory neurons and thereby impedes enhancement of *in vivo* vagal discharges induced by hyperoxia and hypoxia. The results suggest a new O_2-sensing mechanism mediated by TRPA1.

Molecular oxygen plays a paradoxical role in life on the Earth. O_2, the engine of life, is essential for cellular respiration in all aerobic organisms[1]. However, O_2 also exerts toxicity through the production of reactive oxygen species (ROS), causing aging, respiratory disorders and eventually death in a high-O_2 (hyperoxic) environment[1]. Because of the ambivalent physiological nature of O_2, aerobic life forms must adapt to hyperoxia and hypoxia (low-O_2 environment) by sensing surrounding O_2 availability and by transmitting this information to effector systems.

In mammals, the carotid bodies, located near the carotid artery bifurcations, and brainstem catecholaminergic neurons detect changes in partial O_2 pressure (PO_2) in arterial blood[2,3]. With regard to the mechanisms underlying O_2 sensing in the carotid bodies, it is known that BK_{Ca}, TASK and K_V K^+ channels are involved in arterial O_2 sensing[2,4]. Hypoxia inhibits K^+ channels through several mechanisms, such as carbon monoxide production by hemeoxygenase and intracellular ATP depletion to depolarize glomus cells, which lead to the activation of voltage-dependent Ca^{2+} channels, exocytosis and the excitation of carotid sinus nerves; hyperoxia, on the other hand, reduces depolarization and inhibits exocytosis[2,4]. Sensory and vagal afferent neurons, which project nerve endings throughout the body, have also been proposed to detect hypoxia in organs such as the airway, lungs and heart under ischemia and other conditions of low O_2 supply[5–8]. Hypoxia detection by sensory and vagal neurons remains elusive[8]. In terms of hyperoxia, *Caenorhabditis elegans* has been reported to have a strong ability to avoid hyperoxia through detection by sensory neurons[9]. Furthermore, insects breathe discontinuously to avoid O_2 toxicity in hyperoxia[10]. However, the physiological relevance of hyperoxia sensing through sensory systems is less established in vertebrates, including mammals, than in invertebrates. Therefore, it is extremely important to seek hyperoxia-sensing molecular processes in vertebrate sensory systems.

The *Drosophila* TRP protein and its homologs form cation channels activated by sensing diverse stimuli from the extracellular environment and from inside the cell[11,12]. Recently, a class of TRP channels has been demonstrated to act as cell sensors for changes in redox status[13–16]. Certain members of the TRPC and TRPV subfamilies, including TRPC5 and TRPV1, are activated by nitric oxide, oxidants and reactive disulfides through modification of cysteine free sulfhydryl groups[14]. Oxidative cysteine modification by pungent compounds and inflammatory mediators[17–20] are important triggers of TRPA1 activation, as are noxious cold (<17 °C)[21] and other stimulants such as caffeine[22] and infrared[23]. Notably, like polymodal receptors for noxious stimuli at nerve endings in sensory and vagal afferent neurons[21,24–26], TRPV1 and TRPA1 sense endogenous algesic substances and environmental irritants, including oxidants throughout the body, to evoke defensive responses such as pain, coughing and changes in respiration pattern[17,21,24,25,27]. Considering the unique redox reactivities of oxidizing chemical species such as O_2, it is interesting to examine whether particular redox-sensitive TRP channels sense specific ranges of redox status.

Here our systematic chemical-biological evaluation of the redox sensitivity of TRP cation channels reveals that TRPA1 critically contributes to O_2-sensing mechanisms in sensory and vagal afferent neurons. Whereas PHDs exert O_2-dependent inhibition on TRPA1 activity in normoxia, direct O_2 action overrides the inhibition via the strong sensitivity of TRPA1 to cysteine-mediated oxidation in hyperoxia. In hypoxia, TRPA1 is activated through relief from the same PHD-mediated inhibition.

RESULTS

High oxidation sensitivity underlies O_2 sensing of TRPA1

Using a congeneric series of reactive disulfides, we systematically compared the responses of redox-sensitive TRP channels to electrophiles to evaluate the oxidation sensitivities of these channels

[1]Department of Synthetic Chemistry and Biological Chemistry, Graduate School of Engineering, Kyoto University, Kyoto, Japan. [2]Department of Technology and Ecology, Hall of Global Environmental Studies, Kyoto University, Kyoto, Japan. [3]Advanced Biomedical Engineering Research Unit, Kyoto University, Kyoto, Japan. [4]Department of Physiology, Graduate School of Medical and Dental Sciences, Kagoshima University, Kagoshima, Japan. [5]Core Research for Evolutional Science and Technology, Japan Science and Technology Agency, Tokyo, Japan. [6]Division of Pathology, National Ureshino Hospital, Ureshino, Japan. [7]Vesalius Research Center, Catholic University of Leuven, Leuven, Belgium. [8]Vesalius Research Center, Flanders Institute for Biotechnology, Leuven, Belgium. [9]Department of Respiratory Care and Sleep Control Medicine, Graduate School of Medicine, Kyoto University, Kyoto, Japan. [10]Department of Molecular Pharmacology, Graduate School of Pharmaceutical Sciences, Kyoto University, Kyoto, Japan. *e-mail: mori@sbchem.kyoto-u.ac.jp

quantitatively (**Fig. 1a**,**b**)[28]. A strong dependence of the redox potentials on substituents (**Fig. 1a**) suggests that the changes in the electron density distribution of the aromatic ring caused by the presence of substituents affect the reduction propensity of the disulfide bond, thus indicating that redox potential is an excellent index of the electrophilicity of reactive disulfides as electron acceptors (as described in Methods). Indeed, plotting increases of intracellular Ca^{2+} concentration ($[Ca^{2+}]_i$) in human embryonic kidney (HEK) 293 cells expressing recombinant TRPs against redox potentials of reactive disulfide stimuli revealed positive correlations between these parameters and threshold redox potentials (*x* intercepts) for respective TRPs (**Fig. 1c**). This observation strongly indicates that respective redox-sensitive TRP channels have a characteristic redox sensitivity. Among the TRPs tested, only TRPA1 responded to an inert electrophile, diallyl disulfide (redox potential = –2,950 mV), thus revealing that TRPA1 had the highest sensitivity to reactive disulfides. When an inert oxidant O_2 (redox potential = –2,765 mV) was tested, only TRPA1 responded to hyperoxic solution, in an O_2 concentration-dependent manner (as described in Methods) (**Fig. 1d**,**e**), although O_2 differs from reactive disulfides

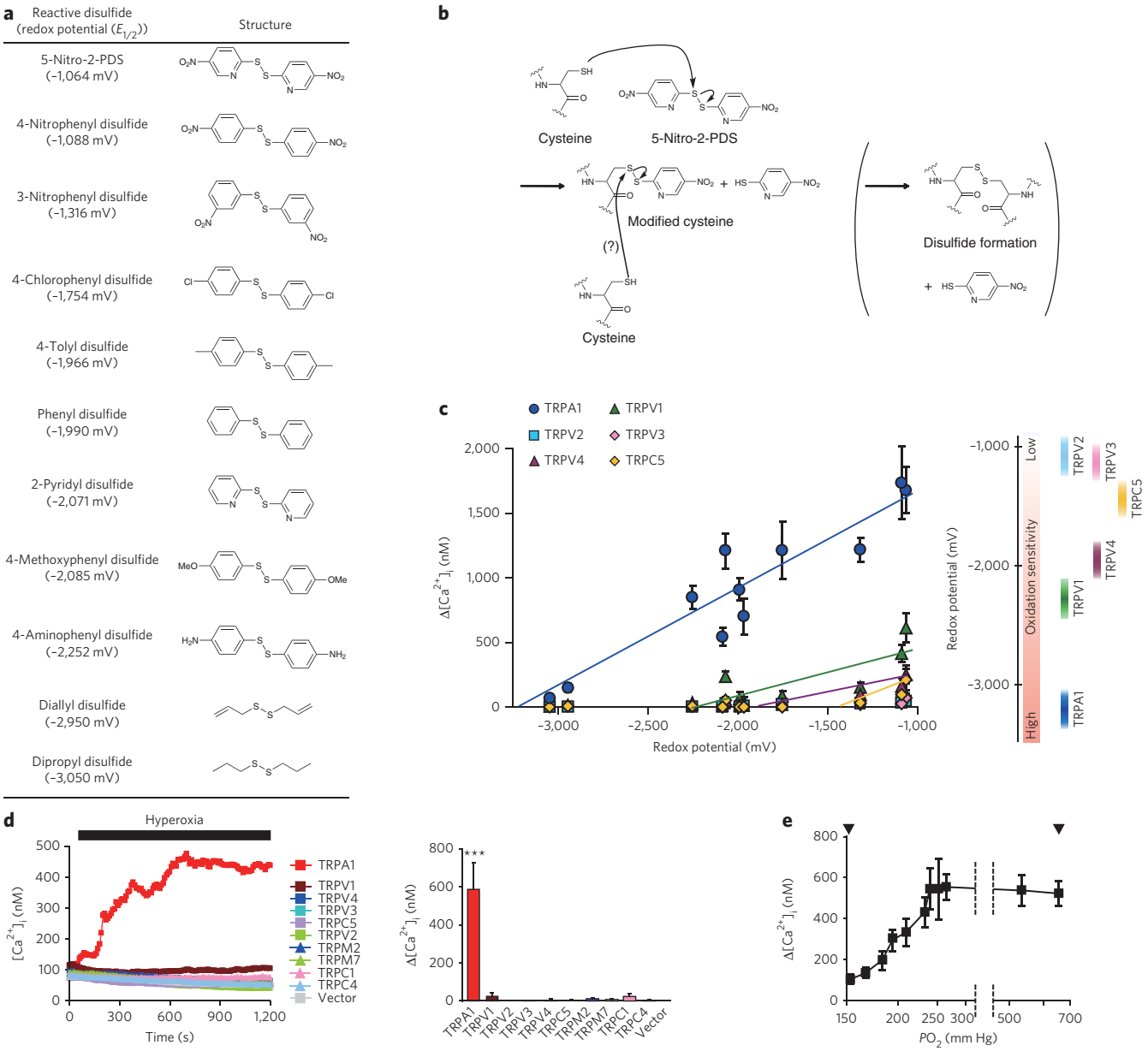

Figure 1 | The prominent oxidation reactivity confers O_2 sensitivity on TRPA1. (**a**) Redox potentials ($E_{1/2}$) of reactive disulfides determined by rotating disk-electrode voltammetry. $E_{1/2}$ values of 5 mM reactive disulfides dissolved in dehydrated DMSO are defined as the midpoint of the rise of current in voltammogram. Compounds with less negative redox potentials have stronger electrophilicity. (**b**) The chemical mechanism underlying the action of a reactive disulfide compound, 5-nitro-2-PDS, on cysteine sulfhydryls. (**c**) Left, oxidation sensitivity of TRP channels. Plots of maximum rises in $[Ca^{2+}]_i$ ($\Delta[Ca^{2+}]_i$), induced by 10 μM of the reactive disulfides (shown in **a**) in HEK 293 cells expressing redox-sensitive TRP channels, against redox potentials of respective substances (n = 13–33). Data points are fit to straight lines by the least-squares method. Right, threshold redox potentials for activation of respective TRP channels. (**d**) $[Ca^{2+}]_i$ rises evoked by hyperoxic solution (86% O_2) in HEK 293 cells expressing redox-sensitive TRP channels. Averaged time courses and $\Delta[Ca^{2+}]_i$ (n = 16–40). ***P < 0.001 compared to vector. (**e**) The relationship between PO_2 and maximum Ca^{2+} responses mediated by TRPA1 (n = 24–41). In examining *in vitro* cellular response to O_2, dissolved PO_2 measured in normoxic (left arrowhead) and hyperoxic solutions (right arrowhead) are 152 ± 1 mm Hg (20% O_2) and 655 ± 32 mm Hg (86% O_2), respectively. Data points are mean ± s.e.m.

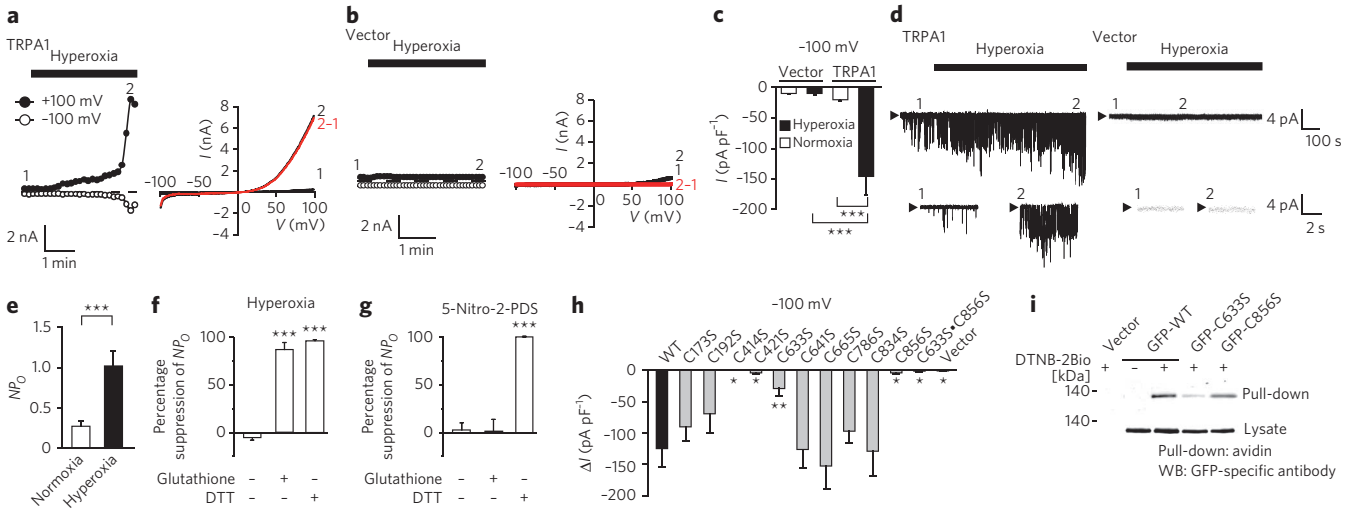

Figure 2 | O_2 directly activates TRPA1 through cysteine modification. (**a**,**b**) Representative time courses of whole-cell currents recorded at +100 and −100 mV under ramp clamp in hyperoxia in TRPA1- (**a**) or vector-transfected HEK 293T cells (**b**). Corresponding *I-V* relationships at the time points 1 and 2 and those of evoked currents (2–1) are shown. (**c**) Peak current densities in normoxia and hyperoxia (n = 6–18). ***P < 0.001. (**d**) Single-channel activities evoked by hyperoxia at −60 mV in inside-out patches excised from TRPA1- or vector-transfected HEK 293T cells. Time-expanded current traces before (1) and during (2) application are also shown. Arrowheads represent the closed state. (**e**) Averages of NP_O (N, number of channels; P_O, open probability) representing single TRPA1 channel activity in normoxia and hyperoxia (n = 20–35). (**f**,**g**) Percentage suppression of hyperoxia-induced (**f**) or 10 μM 5-nitro-2-PDS-induced NP_O of TRPA1 (**g**) by 5 mM reduced glutathione and 10 mM DTT at −60 mV in inside-out patches in HEK 293 cells (n = 5–23). Representative current traces are in **Supplementary Figure 3g**,**j**. ***P < 0.001 compared to cells maintained in hyperoxia or 5-nitro-2-PDS without the agents. (**h**) Changes in current density evoked by hyperoxia (ΔI) for TRPA1 cysteine mutants (n = 5–18). *P < 0.05 and **P < 0.01 compared to wild type (WT). Data points are mean ± s.e.m. (**i**) Effects of mutations C633S and C856S on DTNB-2Bio incorporation into TRPA1 proteins. Western blotting (WB) of total lysates indicates comparable TRPA1 expression (lysate). Full gels and blots are in **Supplementary Figure 6c**.

in that it snatches an electron from a cysteine sulfhydryl group rather than electrophilically attacking the group[29]. Hyperoxia-induced Ca^{2+} responses were suppressed by the TRPA1-specific blocker AP-18 (ref. 30) and by the absence of extracellular Ca^{2+} in TRPA1-expressing HEK 293 cells, indicating that TRPA1 mediates Ca^{2+} entry in response to hyperoxia (**Supplementary Results**, **Supplementary Fig. 1a**,**b**). Other redox-sensitive TRPs (TRPC1, TRPC4, TRPM2 and TRPM7)[14] that by themselves do not respond to reactive disulfides, such as 5-nitro-2-pyridyl disulfide (5-nitro-2-PDS; 10 μM), failed to respond to hyperoxia (**Fig. 1d**).

TRPA1 responses were sustained when switched back to normoxia (20% O_2) after induced conditions of hyperoxia (86% O_2 for 19 min) (**Supplementary Fig. 1a**). The ROS scavenger *N*-acetylcysteine (NAC) or the reducing agent dithiothreitol (DTT), but not the nitric oxide synthase inhibitor N^G-nitro-L-arginine methyl ester (L-NAME), reversed the TRPA1 response during readministration of normoxia. TRPA1 responses were also reversed in normoxia after exposure to mild hyperoxia at a lower O_2 concentration (28%) or to hyperoxia (86% O_2) for a shorter time period (5 min), but they were not reversed after exposure to 5-nitro-2-PDS with the same time protocol (**Supplementary Fig. 1c–e**). The observed reversibility was unaffected by NAC, DTT or L-NAME (**Supplementary Fig. 1d**). Diphenylene iodonium, a potent inhibitor of ROS-producing enzymes, failed to affect hyperoxia-induced TRPA1 responses (**Supplementary Fig. 1f**), suggesting that O_2 action is specifically directed toward cysteine residues. Thus, TRPA1 during activation by hyperoxia may take at least two oxidized states, which are distinguished by reversibility in normoxia after hyperoxia.

In TRPA1-expressing HEK 293T cells, hyperoxia dramatically increased whole-cell currents that were inhibited by AP-18 and DTT (**Fig. 2a–c** and **Supplementary Fig. 2**). Hyperoxia-activated currents showed a reversal potential (E_{rev}) characteristic of nonselective cationic channels (E_{rev} = 2.2 ± 0.9 mV, n = 37). Single-channel currents were significantly enhanced by hyperoxic solution applied from the intracellular side of cell-free, excised inside-out patches at a holding potential (V_h) of −60 mV (**Fig. 2d**,**e**). Unitary conductance was 97.3 ± 2.0 pS at −80 to +20 mV and 180.6 ± 10.7 pS at +40 to +80 mV, as previously reported[26], and the probability that the channels were open ('open probability') was reduced by AP-18 and DTT (**Supplementary Fig. 3a–d**). Single-channel currents were also enhanced by hyperoxic solution applied from the extracellular side of cell-free excised outside-out patches (**Supplementary Fig. 3e**,**f**). Thus, TRPA1 is unique in having a prominent susceptibility to cysteine oxidation that allows it to be directly activated by the weak oxidant O_2 to function as a hyperoxia sensor.

In inside-out patches, single-channel currents induced by relatively short periods of hyperoxia (2 min) were maintained after readministration of normoxia but were reversed by the reduced form of intracellular antioxidant glutathione and DTT (**Fig. 2f** and **Supplementary Fig. 3g**). This observation is consistent with the reversal of hyperoxia-induced single-channel currents by normoxia in cell-attached patches, which maintains intact cellular configuration (**Supplementary Fig. 3h**,**i**). 5-nitro-2-PDS-induced single-channel currents were suppressed by DTT but not by glutathione (**Fig. 2g** and **Supplementary Fig. 3j**). Thus, glutathione-sensitive oxidation of cysteine residues is likely to be involved in TRPA1 activation by hyperoxia.

TRPA1 channel responses showed a characteristic time course: the initial gradually rising phase followed by the second rapidly rising phase (**Fig. 2a** and **Supplementary Fig. 4**). In measurements made using whole-cell patches, the second phase was followed by a gradual decrease that was not seen when other measurement methods were used. This may have been caused by intracellular dialysis of the Ca^{2+} chelator BAPTA via the pipette solution: extracellular Ca^{2+}, which is known to control TRPA1 activity by permeating into the cell[26] (**Supplementary Fig. 4c**,**e**), is absorbed rapidly by BAPTA, which suppresses the global $[Ca^{2+}]_i$ level at

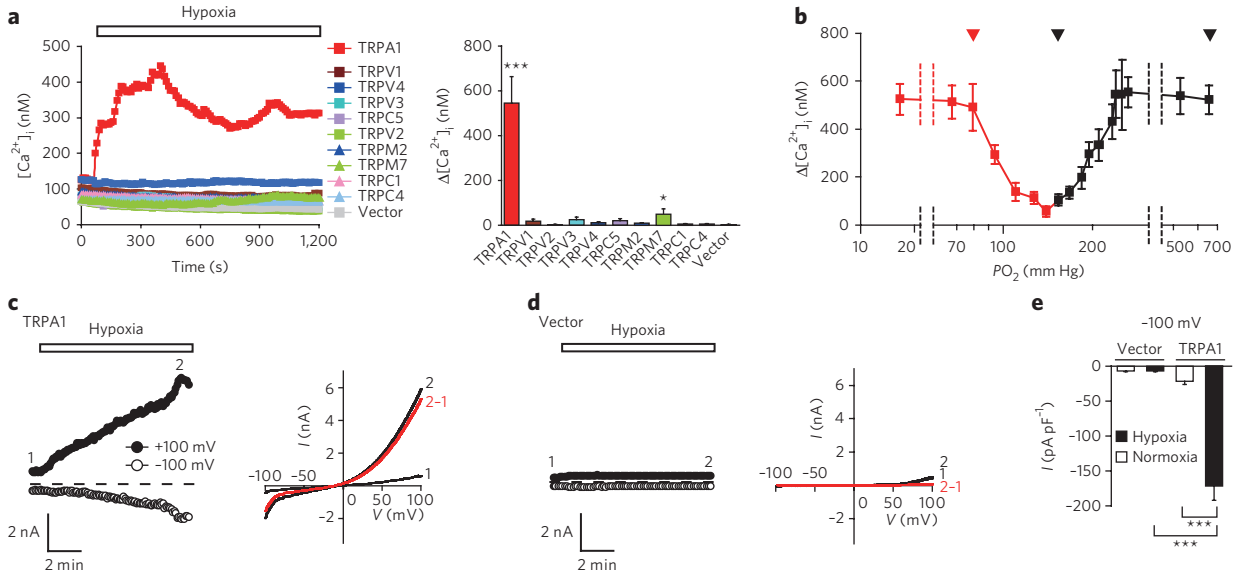

Figure 3 | Hypoxia activates TRPA1. (**a**) $[Ca^{2+}]_i$ rises evoked by hypoxic solution in HEK 293 cells expressing redox-sensitive TRP channels. Dissolved PO_2 measured in the hypoxic solution is 79 ± 3 mm Hg (10% O_2). Averaged time courses and $\Delta[Ca^{2+}]_i$ (n = 20–37). *P < 0.05 and ***P < 0.001 compared to vector. (**b**) The relationship between PO_2 and $\Delta[Ca^{2+}]_i$ mediated by TRPA1 (n = 21–41). Arrowheads indicate, from left to right, PO_2 values for hypoxia, normoxia and hyperoxia. (**c**,**d**) Representative time courses of outward and inward whole-cell currents in hypoxic solution in HEK 293T cells transfected with TRPA1 (**c**) or vector (**d**). Corresponding I-V relationships at the time points 1 and 2 and those of evoked currents (2–1) are also shown. (**e**) Peak current densities at −100 mV in normoxic and hypoxic solutions (n = 4–8). ***P < 0.001. Data points are mean ± s.e.m.

30 nM and localizes $[Ca^{2+}]_i$ elevation near the inner mouth of TRPA1. By contrast, global $[Ca^{2+}]_i$ increases may sustain TRPA1 activity in $[Ca^{2+}]_i$ measurements and cell-attached mode.

Cysteine residues responsible for hyperoxia sensing of TRPA1

We mutated 29 individual cysteine residues in human TRPA1 to serines and tested the responsiveness of these mutant clones. Compared to the wild type, mutants C173S, C192S, C414S, C421S, C633S, C641S, C665S, C786S, C834S and C856S showed significantly (P < 0.0007) suppressed responses to hyperoxia as well as to diallyl disulfide (10 μM), which has a redox potential similar to that of O_2 (**Supplementary Fig. 5a**,**b**). C414S, C421S, C786S and C834S are likely to have deleterious effects on channel function because they significantly (P < 0.012) suppressed responses to 100 μM 2-aminoethyl diphenylborinate (2-APB) (**Supplementary Fig. 5c**), which normally activates TRPA1 independently of cysteine modification[18]. The mutants with impaired responses to hyperoxia were further assessed by the patch-clamp method at fixed membrane potentials and under a defined and optimized intracellular composition using pipette solution containing polytriphosphate (10 mM) and Ca^{2+} (30 nM), which sensitize activity and prevent inactivation of TRPA1, respectively[26,31]. In addition to the nonfunctional mutants, C633S, C856S and the double mutant C633S C856S showed severely suppressed hyperoxia-induced currents, suggesting that Cys633 and Cys856 are the main target sites of O_2 in hyperoxia (**Fig. 2h** and **Supplementary Fig. 5a**,**d**). These mutants required stronger reactive disulfides, such as 5-nitro-2-PDS and 4-nitrophenyl disulfide, at higher concentrations for full activation compared to wild type (**Supplementary Fig. 5e–h**). That TRPA1 responses to the membrane-impermeable reactive disulfide 5,5′-dithiobis(2-nitrobenzoic acid) (DTNB) were induced only in the presence of a detergent, F-127, and were suppressed significantly (P < 0.0013) by C633S and C856S mutations (**Supplementary Fig. 6a**,**b**) supports the cytoplasmic disposition of Cys633 and Cys856. The incorporation of DTNB-2Bio, the DTNB derivative with two biotin groups attached to permit detection[14], into green fluorescent protein–tagged TRPA1 (GFP-TRPA1) was abolished by the C633S mutation but not by C856S (**Fig. 2i** and **Supplementary Fig. 6c**). Notably, transfection of the wild type with the C633S C856S construct at the same amount (1 μg per 10^5 cells) nearly abolished hyperoxia-induced responses but enhanced those induced by 2-APB (**Supplementary Fig. 7**), raising the possibility that all four TRPA1 subunit proteins comprising tetrameric channel complexes[11,12] have to carry oxidizable Cys633, Cys856 or both in responding to hyperoxia. These findings suggest that the free sulfhydryls of Cys633 and Cys856 act as nucleophiles that directly attack electrophiles such as O_2 and reactive disulfides, and this oxidative modification is maintained stably in Cys633 in TRPA1 activation (**Fig. 1b**).

Our single-channel recording in cell-excised membrane patches suggests the role of glutathione in the regulation of hyperoxia-induced TRPA1 activation (**Fig. 2f** and **Supplementary Fig. 3g**). In fact, glutathionylation of TRPA1 detected in normoxia was augmented in hyperoxia after 5 min but became undetectable after 20 min (**Supplementary Fig. 8a**). The disruption of glutathionylation in the C633S C856S mutant implied that there are changes that occur in oxidative modifications at Cys633 and Cys856 during hyperoxia that affect glutathione sensitivity. Notably, when glutathione was perfused via patch pipette solution, hyperoxia-induced whole-cell currents were nearly abolished in the cysteine mutants that showed impaired responses to hyperoxia in $[Ca^{2+}]_i$ measurements but showed intact responses to 2-APB (**Supplementary Fig. 8b**; compare to **Fig. 2h**). Thus, Cys173, Cys192, Cys641, Cys665, Cys786 and Cys834 may protect O_2 reactivity of Cys633 and Cys856 from glutathione, exerting an antioxidant action to reverse TRPA1 activation by O_2.

Central roles of PHDs in hypoxia sensing of TRPA1

Notably, cysteine oxidation is not the only mechanism that underlies O_2 sensing in TRPA1 channels. Indeed, hypoxic solutions prepared by bubbling with N_2 gas induced robust TRPA1 responses; TRPA1 activation showed an inverted bell-shaped O_2-dependence curve with a minimum at the PO_2 of 137 mm Hg (18%), which is slightly below the atmospheric PO_2 of 152 mm Hg (20%) (**Fig. 3a**,**b**), regardless of the presence of bicarbonate and CO_2 (**Supplementary Fig. 9a**). Such O_2 dependence enabled TRPA1 to respond to subtle

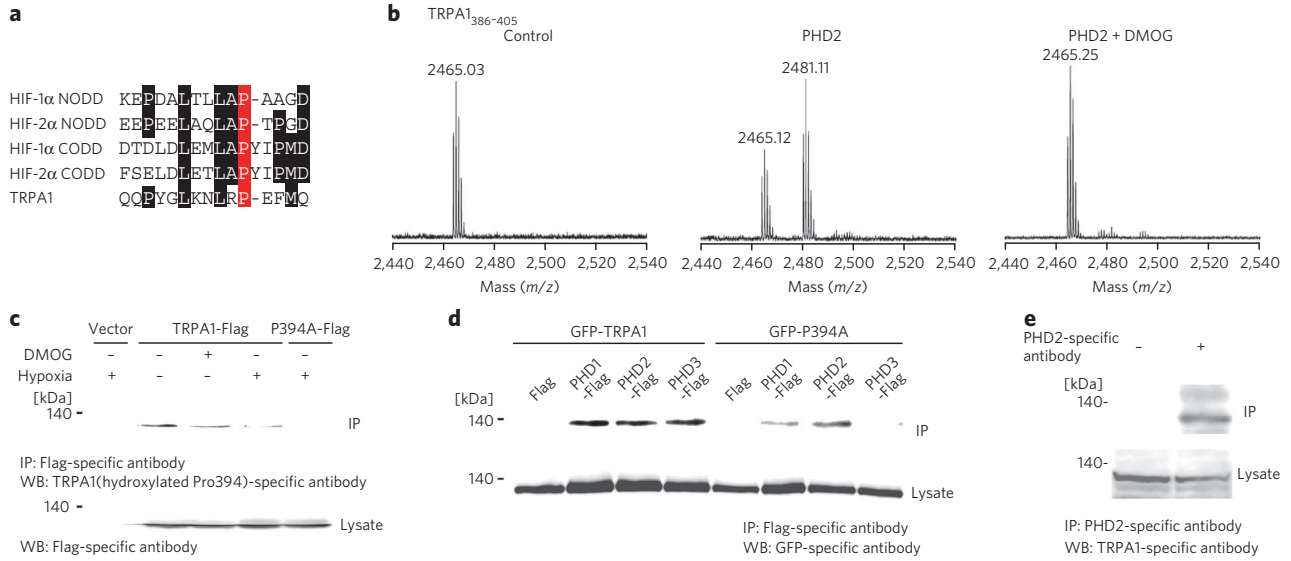

Figure 4 | TRPA1 protein is susceptible to proline hydroxylation by PHDs. (**a**) Alignment of amino acid residues 384–398 of human TRPA1 with conserved prolyl hydroxylation motif within N-terminal and C-terminal O_2-dependent degradation domain (NODD and CODD, respectively) of HIF-1α and HIF-2α. (**b**) Mass spectrometry analysis of TRPA1 peptides incubated with purified recombinant PHD2. Mass increase of 16 Da by PHD2 in the $TRPA1_{386–405}$ peptide is abolished by 3 mM DMOG. (**c**) Hydroxylated Pro394 of TRPA1 is detectable under normoxia but is reduced under hypoxia. TRPA1-Flag–expressing HEK 293 cells are treated with hypoxia for 20 min or 3 mM DMOG for 3 h. Immunoprecipitates (IPs) with antibody to Flag are subjected to western blotting with antibody to TRPA1(hydroxylated Pro394). (**d**) Coimmunoprecipitation of GFP-TRPA1 or GFP-P394A with PHD1–PHD3. IPs with Flag-specific antibody are subjected to western blotting with antibody to GFP. (**e**) Coimmunoprecipitation of native TRPA1 with PHD2 from DRG extract. In **c**–**e**, full gels and blots are available in **Supplementary Figures 10d**,**e** and **11b**.

changes (from 18% to 20% O_2) in the physiological range of PO_2 at sea level, as further described in the Discussion (**Supplementary Fig. 9b**). Hypoxia-induced TRPA1 responses were suppressed by AP-18 and the absence of extracellular Ca^{2+}, indicating that TRPA1 mediates Ca^{2+} entry in response to hypoxia (**Supplementary Fig. 9c**,**d**). Other redox-sensitive TRPs failed to respond to hypoxia except for TRPM7, which elicited marginal responses[16] (**Fig. 3a**). Hypoxia markedly increased whole-cell TRPA1 currents inhibited by AP-18 (**Fig. 3c**–**e** and **Supplementary Fig. 9e**,**f**). Hypoxia-activated TRPA1 currents showed E_{rev} characteristic of nonselective cation channels (E_{rev} = 1.7 ± 0.6 mV; n = 34). That single-channel currents were not enhanced by hypoxic solution in excised inside-out patches (**Supplementary Fig. 9g**,**h**) suggests that intracellular components are required for TRPA1 activation in hypoxia.

The PHD family comprises subtypes PHD1, PHD2 and PHD3, which, as a result of their absolute requirement upon O_2 as a cofactor for enzymatic activity, are central to hypoxia-sensing pathways leading to activation of hypoxia-inducible factor 1α (HIF-1α)[32,33]. Importantly, because Michaelis constant (K_M) values of PHDs for O_2, representing the substrate concentration at which half of the enzyme active sites are occupied, are close to the atmospheric O_2 concentration, physiological reductions in O_2 concentration result in a decrease in protein hydroxylation by PHDs. Notably, alignment of the consensus sequences for the prolyl hydroxylation motif[32,33] with the amino acid sequence of TRPA1 revealed conservation of the flanking amino acid residues of Pro394 in the N-terminal cytoplasmic ankyrin repeat of TRPA1 (**Fig. 4a**). When PHD2, the ubiquitous PHD isoform[32,33], was incubated together with the $TRPA1_{386–405}$ peptide substrate that includes the motif, mass spectrometry analysis of the resultant peptide product showed a mass increase of 16 Da that is consistent with hydroxylation of proline residues (**Fig. 4b**). This mass increase was undetectable in $TRPA1_{386–405}$ incubated with the pan-hydroxylase inhibitor dimethyloxalylglycine (DMOG), in $TRPA1_{386–405}$P394A and in $TRPA1_{983–1002}$ (**Fig. 4b** and **Supplementary Fig. 10a**,**b**). Prolyl hydroxylation, which was detected using antibody against a synthetic TRPA1 subfragment carrying hydroxylated Pro394, was suppressed by DMOG, hypoxia and the P394A mutation (**Fig. 4c** and **Supplementary Fig. 10c**,**d**). Furthermore, GFP-TRPA1 immunoprecipitated together with Flag-tagged PHDs 1–3, which were reduced in GFP-P394A (**Fig. 4d** and **Supplementary Fig. 10e**). Interaction between native PHD2 and TRPA1 proteins was confirmed by coimmunoprecipitation using mouse dorsal root ganglia (DRG) cell extract (**Fig. 4e** and **Supplementary Fig. 11**).

Recombinant TRPA1 channels were activated by inhibition of endogenous PHDs by DMOG in HEK 293 cells (**Fig. 5a**,**b** and **Supplementary Fig. 12**). The DMOG-induced TRPA1 activity that was suppressed by intracellular application of purified PHD2 through patch pipette solution (**Fig. 5b**–**d**) suggests that an increase in the absolute quantity of DMOG-unbound PHD2 inhibits TRPA1. Overexpression of PHD2 suppressed TRPA1 responses to mild hypoxia (PO_2 at 14%) (**Supplementary Fig. 13**). Furthermore, overexpression of catalytically dead mutants of PHD1 (PHD1-Mut), PHD2 (PHD2-Mut) and PHD3 (PHD3-Mut), each of which immunoprecipitated together with GFP-TRPA1, elevated basal $[Ca^{2+}]_i$ indicative of constitutive TRPA1 activation and abolished TRPA1 responses to hypoxia and DMOG (**Fig. 5e**,**f** and **Supplementary Fig. 14a**–**d**). By contrast, the PHD-Muts failed to affect TRPA1 responses to both allyl isothiocyanate (AITC) and hyperoxia (**Supplementary Fig. 14e**,**f**). Co-transfection of siRNAs for PHD1–PHD3 abrogated TRPA1 responses to hypoxia but not to hyperoxia (**Fig. 5g** and **Supplementary Fig. 15**). P394A showed significantly elevated basal activity and abrogated responses to hypoxia and DMOG but not to AITC and hyperoxia (**Fig. 5h** and **Supplementary Fig. 16**). These results suggest that hydroxylation of Pro394 by PHDs inhibits TRPA1 channels in normoxia, whereas a decrease in O_2 concentration diminishes PHD activity, thus relieving TRPA1 from inhibition and ultimately leading to channel activation in hypoxia.

On the other hand, hyperoxia-induced TRPA1 activation was observed even in the presence of excess intracellular PHD2 applied through patch-pipette solution (**Supplementary Fig. 17a**–**d**). The single-channel behaviors of wild-type TRPA1 and the P394A

mutant in hypoxia were compared with those induced by hyperoxia or normoxia using the cell-attached patch-clamp method (**Supplementary Fig. 17e,f** and **Supplementary Table 1**). Open times were fitted to three components with different ranges of time constants: τ_1 = 0.53–3.04 ms, τ_2 = 3.35–22.01 ms and τ_3 = 31.01–136.12 ms. Notably, induction of the open state was significantly (P = 0.000011) enhanced with τ_2 in hypoxia compared to normoxia in the wild type, whereas that observed with τ_1 and τ_2 were similar in normoxia and hypoxia for P394A, suggesting that hydroxylation of Pro394 prevents TRPA1 from dwelling in a state with longer open time (τ_2). Hyperoxia, however, induced open states with τ_1, τ_2 and τ_3 regardless of hydroxylation at Pro394, which is supported by TRPA1 responses to hyperoxia in the presence of DMOG (**Supplementary Fig. 17g**). Therefore, it is quite conceivable that direct O_2 action overrides the PHD-mediated inhibition via the prominent sensitivity of TRPA1 to cysteine-mediated oxidation in hyperoxia.

Protein translocation has been reported to regulate activation of TRP channels, including TRPA1 (refs. 34,35). GFP-TRPA1 showed discontinuous overlaps with the plasma membrane marker DsRed-monomer-F in confocal laser microscopy (**Supplementary Fig. 18a**). Evanescent wave microscopy, which illuminates only the subcellular area from the surface of the cell to a depth of less than 100 nm through total internal reflection fluorescence (TIRF), revealed instantaneous augmentation of the amount of GFP-TRPA1 near the cell surface upon hypoxia (**Fig. 5i,j** and **Supplementary Fig. 18b**). Chlorpromazine (CPZ) and dynasore, inhibitors of

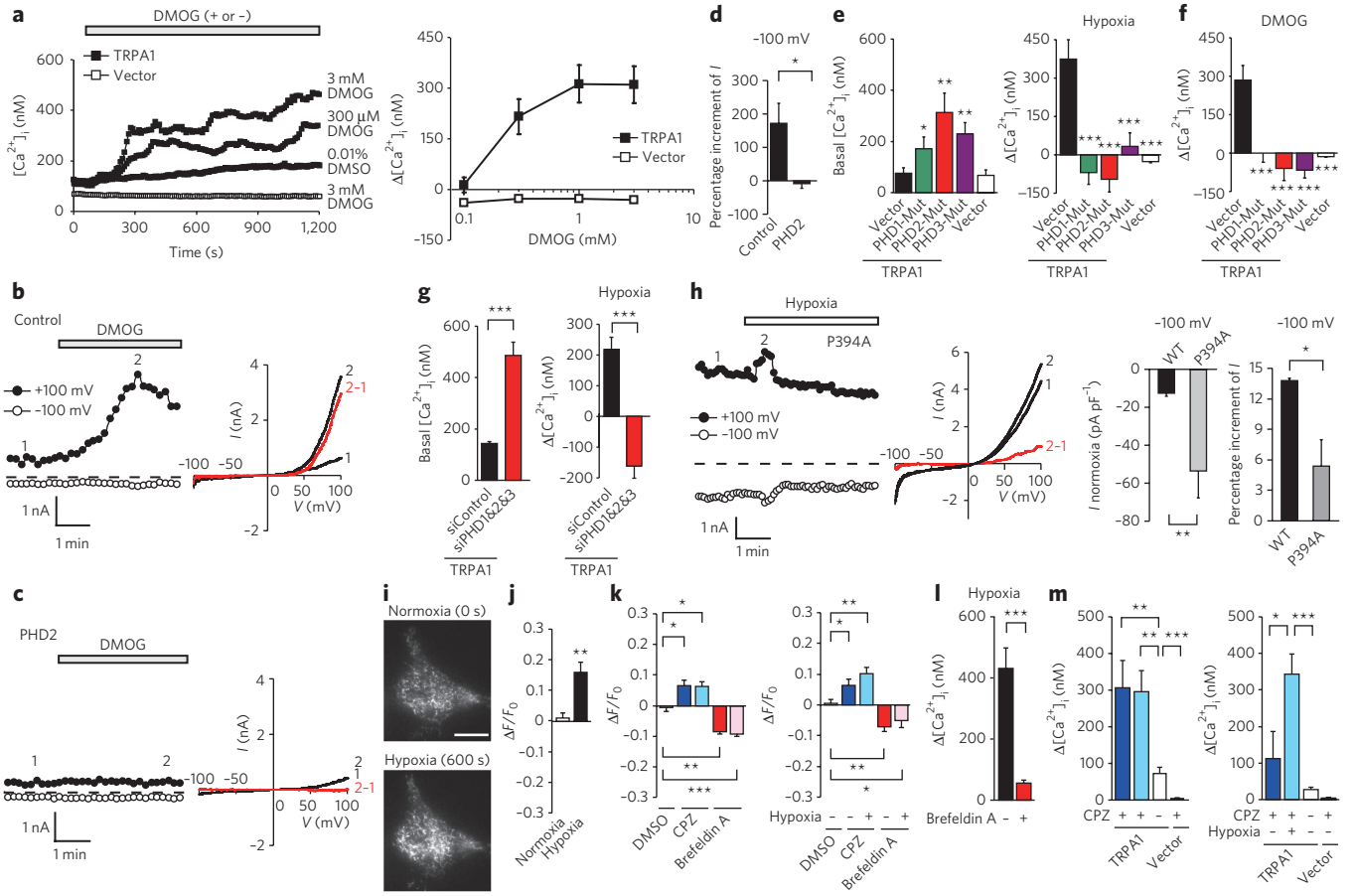

Figure 5 | TRPA1 is activated by relief from O_2-dependent inhibition by proline hydroxylation. (**a**) TRPA1 responses to DMOG. Averaged time courses of $[Ca^{2+}]_i$ changes evoked by DMOG or its vehicle (0.01% DMSO) and dose dependence of average $[Ca^{2+}]_i$ rises during 1,080–1,200 s (n = 22–36). (**b**–**d**) Whole-cell TRPA1 currents evoked by 300 μM DMOG with and without intracellular application of recombinant PHD2 (0.67 μM). Representative time courses and corresponding I-V relationships (**b**,**c**). Percentage increment of peak currents after DMOG administration (n = 7–10) (**d**). (**e**,**f**) TRPA1 responses to hypoxia (**e**) and 300 μM DMOG (**f**) are affected by co-transfection of PHD1-Mut, PHD2-Mut or PHD3-Mut. Basal $[Ca^{2+}]_i$ (**e**) and average $[Ca^{2+}]_i$ rises during 1,020–1,140 s of stimulation (**e**,**f**) (n = 13–50). $^*P < 0.05$, $^{**}P < 0.01$ and $^{***}P < 0.001$ compared to co-transfection with vector. (**g**) TRPA1 responses to hypoxia after treatment with combined siRNAs for PHDs (siPHD1&2&3). Basal $[Ca^{2+}]_i$ and average $[Ca^{2+}]_i$ rises during 1,020–1,140 s of stimulation (n = 80–147). (**h**) Representative time courses of whole-cell P394A currents in hypoxia. Corresponding I-V relationships. Peak current densities in normoxia (n = 23–38) and percentage increment of the peak current in hypoxia relative to that in normoxia (n = 6–24). (**i**,**j**) Cell-surface expression of GFP-TRPA1 observed by TIRF microscopy is enhanced by hypoxia. Representative images are shown in (**i**). Scale bar, 10 μm. (**j**) Average fluorescence changes in TIRF images ($\Delta F/F_0$) during 680–780 s of stimulation (n = 12–20). (**k**) Protein translocation inhibitors affect $\Delta F/F_0$. After 3-min incubation with 5 μg ml^{-1} CPZ, 100 μM brefeldin A or their vehicle (0.1% DMSO), cells are exposed to hypoxia. Average $\Delta F/F_0$ measured 0–50 s before and 500–600 s after start of hypoxia (light blue and red correspond to time course data, indicated by open squares, in **Supplementary Fig. 18d**) or measured with the same timing as in control experiment (corresponding to blue and red solid squares in **Supplementary Fig. 18d**) are shown (n = 12–16). (**l**) Brefeldin A inhibits hypoxia-induced TRPA1 responses. Three hours before and during hypoxia, cells are incubated with 100 μM brefeldin A. $\Delta[Ca^{2+}]_i$ is shown (n = 27–28). (**m**) TRPA1 responses to CPZ. After 7 min incubation with 1 μg ml^{-1} CPZ or its vehicle (0.1% DMSO), cells are exposed to hypoxia. $\Delta[Ca^{2+}]_i$ measured 0–420 s before and after start of hypoxia (light blue; blue open squares indicate the corresponding time course in **Supplementary Fig. 18k**) or measured at the same timing in control (blue; blue solid squares indicate the corresponding time course in **Supplementary Fig. 18k**) are shown (n = 17–33). $^*P < 0.05$, $^{**}P < 0.01$ and $^{***}P < 0.001$. Data points are mean ± s.e.m. Corresponding time course data for **e**–**g**, **j** and **l** are in **Supplementary Figures 14c**,**d**, **15b** and **18b**,**j**.

clathrin-dependent endocytosis, and brefeldin A, an inhibitor of ER–Golgi exocytotic protein translocation, revealed insertion and internalization of GFP-TRPA1 in the plasma membrane, respectively (**Fig. 5k** and **Supplementary Fig. 18c–e**). The observed internalization and insertion events of GFP-TRPA1 were unaffected by hypoxia. In this protocol, GFP-TRPA1 most likely exists in a hydroxylated form in the plasma membrane after its insertion is inhibited by brefeldin A. Notably, plasma membrane localization of GFP-TRPA1 is enhanced by DMOG (**Supplementary Fig. 18f**). The data suggests that internalization of TRPA1 with unmodified Pro394 is decelerated in hypoxia because insertion was unaffected in hypoxia (**Fig. 5k** and **Supplementary Fig. 18d,e**). Filipin, an inhibitor of caveolae-mediated endocytosis, failed to affect the amount of GFP-TRPA1 that localized in the plasma membrane (**Supplementary Fig. 18g**). Cell-surface labeling experiments support these microscopy data (**Supplementary Fig. 18h,i**). $[Ca^{2+}]_i$ measurements showed that brefeldin A suppressed TRPA1 responses to hypoxia, whereas CPZ and dynasore, but not filipin, induced TRPA1 responses in normoxia (**Fig. 5l,m** and **Supplementary Fig. 18j–m**). Thus, turnover of TRPA1 proteins in the plasma membrane is actively maintained to regulate TRPA1 activity in normoxia and hypoxia, suggesting that insertion of unmodified TRPA1 and internalization of hydroxylated TRPA1 underlie the relief of TRPA1 channel activity from PHD-mediated inhibition.

TRPA1 responses were sustained when switched back to normoxia (20% O_2) after induced conditions of hypoxia (10% O_2 for 19 min) (**Supplementary Fig. 19a**). NAC and DTT but not L-NAME reversed the TRPA1 response during readministration of normoxia. Hypoxia-induced TRPA1 responses were also reversed in normoxia after exposure to hypoxia for a shorter time period (5 min) or mild hypoxia at a higher O_2 concentration (14%) (**Supplementary Fig. 19b,c**). The observed reversibility was unaffected by NAC, DTT or L-NAME. Wash-out of DMOG partially reversed TRPA1 responses (**Supplementary Fig. 19d**), indicating that restoration of PHD activity inhibits TRPA1. Thus, the time and degree of hypoxia preceding normoxia and the amount of ROS present are critical to induce irreversibility of TRPA1 activation in normoxia.

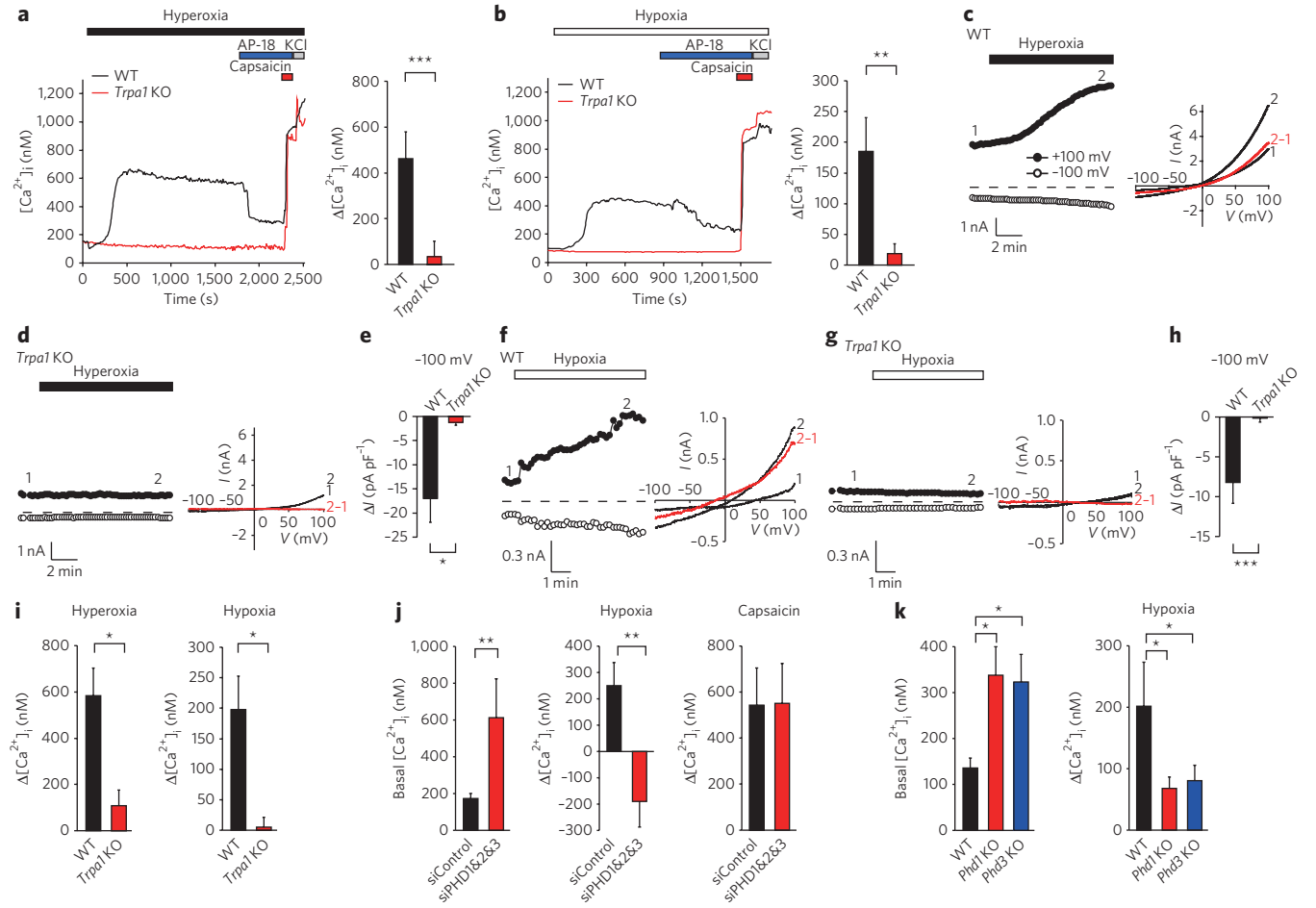

Figure 6 | TRPA1 mediates hyperoxia- and hypoxia-induced cationic currents in vagal and sensory neurons. (**a**,**b**) Hyperoxia- (**a**) and hypoxia-induced Ca^{2+} responses (**b**) are ablated in capsaicin-sensitive *Trpa1* knockout (KO) nodose ganglion neurons as compared to wild type (WT). Representative Ca^{2+} responses evoked in hyperoxia (**a**) or hypoxia (**b**) and by 10 μM AP-18 (0.01% DMSO), 3 μM capsaicin (0.01% DMSO) and 60 mM KCl, and $\Delta[Ca^{2+}]_i$ at 60–1,800 (**a**) or 60–900 s (**b**) (n = 13–46). (**c**–**h**) Whole-cell currents recorded in wild-type and *Trpa1* knockout nodose ganglion neurons. Representative time courses and corresponding I-V relationships in hyperoxia (**c**,**d**) and hypoxia (**f**,**g**). Current densities (ΔI) evoked by hyperoxia (**e**) and hypoxia (n = 16–19) (**h**). (**i**) Ablated Ca^{2+} responses to hyperoxia and hypoxia in capsaicin-sensitive *Trpa1* knockout DRG neurons. $\Delta[Ca^{2+}]_i$ during 0–1,440 s of hyperoxic stimulation and 0–840 s of hypoxic stimulation (n = 12–49). (**j**) Ca^{2+} responses to hypoxia in capsaicin-sensitive DRG neurons treated with siPHD1&2&3. Basal $[Ca^{2+}]_i$ and average $[Ca^{2+}]_i$ rises during 740–840 s of hypoxic stimulation and 0–100 s after start of stimulation with capsaicin (n = 16–27). (**k**) Ca^{2+} responses to hypoxia in capsaicin-sensitive *Phd1* or *Phd3* knockout DRG neurons. Basal $[Ca^{2+}]_i$ and $\Delta[Ca^{2+}]_i$ during 0–840 s of hypoxic stimulation (n = 22–59). $^*P < 0.05$, $^{**}P < 0.01$ and $^{***}P < 0.001$. Data points are mean ± s.e.m. Corresponding time course data for **i**–**k** are in **Supplementary Figures 22e**,**f** and **23d**,**e**.

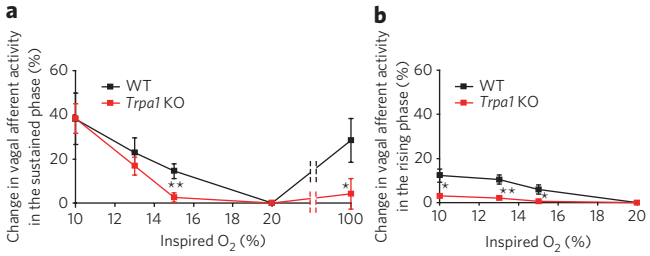

Figure 7 | Defects of discharges in vagal afferents of *Trpa1* knockout mice under systemic hypoxia and hyperoxia. (**a**,**b**) Comparison of percentage changes in rectified and integrated vagal nerve activity in response to inhalation of hypoxic (10%, 13% and 15% O_2) or hyperoxic (100% O_2) gas between wild-type and *Trpa1* knockout mice in the sustained phase (20–30 s) (**a**) or in the rising phase (0–10 s) (**b**) during changes of O_2 availability (n = 4–7). Values denote percentage changes from basal activities recorded during normoxic gas (20% O_2) exposure. Representative tracings of vagal afferent discharges and rectified and integrated vagal nerve activities are shown in **Supplementary Figure 24**. $^*P < 0.05$ and $^{**}P < 0.01$ compared to wild type. Data points are mean ± s.e.m.

Receptor stimulation via phospholipase C (PLC) activates TRPA1 (ref. 36). However, the PLC inhibitor edelfosine failed to affect responses of TRPA1 to hypoxia and hyperoxia (**Supplementary Fig. 20a**,**b**), suggesting that PLC activity is not required for O_2-mediated activation of TRPA1. Activation of TRPA1 through receptor stimulation by bradykinin at low concentrations (1–100 nM) was prominently enhanced by hypoxia (**Supplementary Fig. 20c**). That P394A showed bradykinin-induced responses similar to those observed in hypoxia (**Supplementary Fig. 20c**,**d**) suggests that prolyl hydroxylation is not necessary for activation of TRPA1 via PLC-mediated receptor signaling pathways. Thus, PHD and PLC-mediated receptor signaling pathways may operate independently but can act synergistically to better adapt TRPA1 activation through humoral factors to hypoxia.

Hyperoxia and hypoxia excite peripheral nerves via TRPA1

Like polymodal receptors for noxious stimuli at nerve endings in sensory and vagal afferent neurons[21,26], TRPA1 senses endogenous algesic substances and environmental irritants[17,21,24,27]. Notably, TRPA1 protein was identified by immunohistochemistry in a subset of nodose ganglion neurons projecting to the lung and airway in mice[27] (**Supplementary Fig. 21a**). We tested whether TRPA1 detects changes in O_2 availability in the mouse nodose ganglion (**Fig. 6a–h**), in which cell bodies of vagal nerves are located and PHDs are abundantly expressed (**Supplementary Fig. 21b**). Robust $[Ca^{2+}]_i$ increases were induced by hyperoxia and hypoxia in a subset of cells responsive to 60 mM KCl, which activates voltage-dependent Ca^{2+} channels in neurons regardless of the presence of bicarbonate and CO_2 (**Fig. 6a**,**b** and **Supplementary Fig. 21c–f**). The observation that the majority of hyperoxia- and hypoxia-responsive cells responded to the C fiber-specific sensory irritant capsaicin[27] (**Fig. 6a**,**b**, **Supplementary Fig. 21c**,**d** and **Supplementary Table 2**) suggests that a TRPA1-expressing subset of C fibers senses O_2 availability changes. Whole-cell current amplitudes were also augmented by hyperoxia and hypoxia in nodose neurons (**Fig. 6c**,**f** and **Supplementary Fig. 21g**,**h**). Hyperoxia- and hypoxia-induced currents showed E_{rev} values characteristic of nonselective cation channels (hyperoxia; E_{rev} = 0.9 ± 1.0 mV, n = 31), hypoxia; E_{rev} = −0.8 ± 1.3 mV, n = 15). Ca^{2+} responses and ionic currents induced by hyperoxia and hypoxia were substantially blocked by AP-18 in nodose neurons (**Supplementary Fig. 21c–h**).

Notably, nodose neurons prepared from *Trpa1* knockout mice[37] were largely unresponsive to hyperoxia and hypoxia, but they retained responsiveness to capsaicin and 60 mM KCl (**Fig. 6a–h**). In *Trpa1* knockout mice, it is interesting to note that statistically significant impairments ($P < 0.009$) were observed in responses to hypoxia (10%, 13% and 15% O_2) when capsaicin-sensitive nodose neurons were selected for analyses, but the impairments were observed only in responses to relatively mild hypoxia (15% O_2) when all nodose neurons were subjected to analyses (**Supplementary Fig. 21i**,**j**). DRG neurons from wild-type mice exhibited robust responses to hyperoxia and hypoxia via Ca^{2+} influx blocked by AP-18, while those from *Trpa1* knockout mice showed impaired responses to hyperoxia and hypoxia (**Fig. 6i**, **Supplementary Fig. 22a–h** and **Supplementary Table 2**). *Trpa1* knockout also abrogated ability of DRG to respond to subtle O_2 changes (from 18% to 20%) within the physiological range at sea level (**Supplementary Fig. 22i**). These results suggest that hyperoxia and hypoxia activate native TRPA1 channels in mouse vagal neurons and sensory neurons.

To establish the role of PHDs in activation of native TRPA1 by hypoxia, we used an siRNA strategy for PHD1–PHD3 and *Phd* knockout mice. Abundance of expression was highest in PHD2, followed by PHD1 and PHD3 in DRG and nodose neurons (**Supplementary Fig. 23a**). Antibodies specific to TRPA1 hydroxylated at Pro394 revealed immunostaining localized near the plasma membrane, which showed the position of these proteins relative to the total population of TRPA1 proteins in DRG neurons (**Supplementary Fig. 23b**). Cotransfection of siRNAs for PHD1–PHD3 elevated basal $[Ca^{2+}]_i$ and abolished responses of capsaicin-sensitive DRG neurons to hypoxia (**Fig. 6j** and **Supplementary Fig. 23c**,**d**). In capsaicin-sensitive DRG neurons isolated from *Phd1* and *Phd3* knockout mice[38–40], basal $[Ca^{2+}]_i$ was elevated and responses to hypoxia were suppressed, whereas responses to hyperoxia were intact compared with those of wild-type mice (**Fig. 6k** and **Supplementary Fig. 23e**,**f**). Thus, PHDs are essential for TRPA1 responses to hypoxia.

We evaluated *in vivo* TRPA1 responses that regulate vagal activities under systemic hyperoxia and hypoxia. Exposure of wild-type mice to hyperoxic (100% O_2) or hypoxic (10, 13 and 15% O_2) gas via a tracheal cannula significantly ($P < 0.05$) enhanced discharges of afferents in the cervical vagal trunk and in the superior laryngeal vagal branch innervating the mucosa of the larynx as shown by multifiber neurogram (**Fig. 7** and **Supplementary Figs. 24** and **25**). In *Trpa1* knockout mice, the enhancement of nerve discharges by hyperoxia and mild hypoxia (15% O_2) was abolished, whereas that by severe hypoxia (10% and 13% O_2) was delayed. Basal activity in normoxia (20% O_2) of vagal afferents in *Trpa1* knockout mice was indistinguishable from that in wild-type mice. Thus, the observation that TRPA1 is essential for regulation of discharges in vagal afferents in hyperoxia and mild hypoxia (15% O_2) but plays less critical roles in severe hypoxia (10% or 13% O_2) suggests that other hypoxia-sensitive channels such as K^+ channels contribute to vagal discharges in severe hypoxia[2,4].

DISCUSSION

The present study reveals critical roles of TRPA1 in O_2 sensing of vagal and sensory neurons. TRPA1 is activated by hyperoxia and hypoxia through mechanisms involving cysteine oxidation and proline hydroxylation, respectively.

Our results suggest that free cysteine sulfhydryls are the key to the O_2-sensing ability of TRPA1 in hyperoxia. The high reactivity of Cys633 and Cys856 as electron donors enables TRPA1 to respond to O_2, which is a relatively poor electron acceptor, by overriding the inhibition caused by proline hydroxylation to activate TRPA1. Contribution of multiple cysteine residues to oxidation sensitivity of protein function has also been reported for other proteins[41–43]. Because sensitivities to O_2 and reactive disulfides are reduced efficiently and similarly in single mutants C633S and C856S and are nearly abolished in the double mutant C633S C856S, these cysteine residues are more likely to contribute to

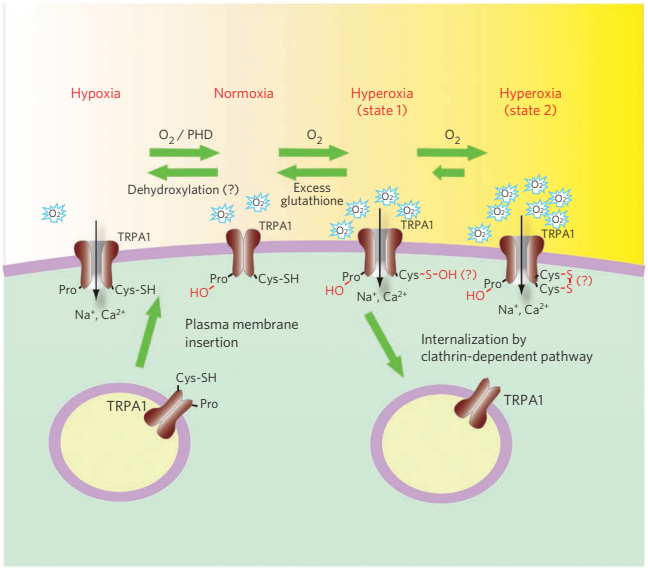

Figure 8 | Molecular mechanism underlying O_2-sensing in TRPA1 channel. PHDs hydroxylate conserved Pro394 within the N-terminal ankyrin repeat of TRPA1 in normoxia, whereas a decrease in O_2 concentrations diminishes PHD activity and relieves TRPA1 from the prolyl hydroxylation, leading to its activation in hypoxia. The relief can be achieved by insertion of unmodified TRPA1 proteins to the plasma membrane or by dehydroxylation through an unidentified molecular mechanism. In hyperoxia, O_2 oxidizes Cys633, Cys856 or both, thereby activating TRPA1. TRPA1 may at least take two oxidized state upon hyperoxia: a relatively unstable oxidized state (state 1) readily reversed by glutathione and a relatively stable oxidized state (state 2). Sulfhydryl group(s) (SH) of the key cysteine residue(s) Cys633, Cys856 or both may be modified to sulfenic acid (S-OH) in the former state of TRPA1, whereas that in the latter state of TRPA1 may form a disulfide bond(s) (S-S). These oxidation mechanisms override the inhibition by prolyl hydroxylation to activate TRPA1.

the same molecular determinant for O_2 sensitivity than to separate sites with characteristic oxidation sensitivities. Importantly, in regard to the activation of TRPA1, our mutation studies suggest that relatively weak electron acceptors such as diallyl disulfide and 4-tolyl disulfide target the same cysteine residues as O_2, whereas strong electron acceptors such as 4-nitrophenyl disulfide and 5-nitro-2-PDS also act on additional cysteine residues (**Supplementary Fig. 5a**,**b**,**f**–**h**). Multiple cysteine residues, different from those described for O_2 sensing, have been identified as sensors of α,β-unsaturated carbonyls[18–20]. The difference is attributable to the different stabilities of the immediate reaction products: O_2 may lead to disulfide bond formation via an unstable oxidized product (**Fig. 8**), whereas α,β-unsaturated carbonyls give stable Michael addition adducts.

The reversibility of TRPA1 activation in normoxia depends on the time and degree of preceding hyperoxia (**Supplementary Fig. 1**). This finding, together with the observed sensitivity of TRPA1 to ROS and antioxidant inhibitors, suggests that a transition of oxidation state is induced in Cys633 and Cys856 (**Fig. 8**): the sulfhydryl groups of Cys633 and Cys856 are initially oxidized by hyperoxia into glutathione-sensitive sulfenic acid and are subsequently converted into relatively stable, glutathione-insensitive disulfide bonds[44]. The dominant inhibitory effect of the C633S C856S mutant implies that oxidation is introduced in all four subunits of the TRPA1 channel complex for activation, although it is unclear whether disulfide bonds are formed intermolecularly or intramolecularly by TRPA1 proteins. Our data also suggest that extracellular Ca^{2+} plays an important role in the later phase of TRPA1 activation[26].

Multiple stimuli activate TRPA1 (refs. 17–24). Our preliminary experiments have suggested that cold-sensitive activation of TRPA1 is in part due to the well-known effect of cold temperature to enhance dissolution of O_2 (data not shown). Zn^{2+}, well known for binding to cysteine residues, activates TRPA1 (ref. 45). Interestingly, in TRPV1, cysteine S-nitrosylation prominently enhances sensitivity to protons[14], which also activate TRPA1 (refs. 20,46). Therefore, redox sensitivity may be coupled with other modes of sensitivity to finely regulate TRPA1, depending on the environment.

In adaptation to hypoxia, elevated amounts of HIF-1α increase red blood cell mass and stimulate new blood vessel growth[33,47]. Prolyl hydroxylation of HIF-1α by PHDs 1–3, which use molecular O_2 and 2-oxoglutarate as substrates, and the subsequent ubiquitination and targeting of HIF-1α to the 26*S* proteasome for degradation control HIF-1α concentrations[32]. Notably, TRPA1 represents the first example of a channel where the activation is controlled by prolyl hydroxylation. PHDs hydroxylate conserved Pro394 within the N-terminus ankyrin repeat of TRPA1 and inhibit TRPA1 channels in normoxia, whereas hypoxia diminishes PHD activity and relieves TRPA1 from inhibition, leading to its activation. Importantly, the O_2 dependence of PHD enzymatic activity is consistent with the importance of PHDs in inhibition of TRPA1 activity: the normoxic O_2 concentration of 200 μM (152 mm Hg) is comparable to the K_M values of 230–250 μM (175–190 mm Hg) by O_2 concentrations for PHDs[33]. TRPA1 inhibition relief can be achieved by rapid insertion of unmodified TRPA1 proteins into the plasma membrane or by dehydroxylation through an unidentified molecular mechanism. Our data, which demonstrate that turnover of TRPA1 proteins is maintained in the plasma membrane and that inhibition of PHDs by DMOG decelerates their internalization (**Fig. 5i**–**m** and **Supplementary Fig. 18**), support the view that insertion of unmodified TRPA1 proteins contributes to instantaneous TRPA1 responses to hypoxia. The different gating behaviors of single TRPA1 channels observed in normoxia and hypoxia (**Supplementary Fig. 17e**,**f** and **Supplementary Table 1**) are more compatible with the notion of TRPA1 channel activation via dehydroxylation in hypoxia, although this data does not necessarily contradict the translocation scenario, in which TRPA1 proteins inserted in the plasma membrane remain dehydroxylated in hypoxia but immediately become hydroxylated in normoxia. The importance of mitochondrial function in triggering hypoxic inhibition of K^+ channels has been suggested because mitochondria consume the majority of O_2 in the cell and control cytosolic O_2 concentration[4]. Depletion of intracellular ATP and production of carbon monoxide by hemeoxygenase have also been suggested to have a role in K^+ channel inhibition[4]. These mechanisms can also contribute to hypoxia-induced activation of TRPA1.

It is known that hypoxia is involved in some pathophysiological reactions such as nociceptive pain in sensory neurons[7,8,48]. For example, chest pain occurs when the heart is exposed to hypoxia caused by coronary artery blockade, disease or inhalation of hypoxic gas, and surgical dissection of cardiac sensory neurons relieves angina[48]. Our observation that hypoxia potently excites DRG neurons in a TRPA1-dependent manner (**Fig. 6i** and **Supplementary Fig. 22**) suggests that hypoxia-activated TRPA1 together with other mechanisms such as K^+ leak[7] may underlie chest pain via cardiac sensory neurons.

The vagal nerve conveys sensory information about the state of the body's organs to the central nervous system in addition to providing output to the various organs in the body. Enhanced discharges in vagal afferents induce respiratory, cardiac and vascular responses[8,48,49]. Chemicals encountered in the airway and lungs are detected by bronchopulmonary C fibers and the superior laryngeal nerve, which is a branch of the vagal nerve[49]. Recently, TRPA1 has been shown to sense environmental irritants, thus initiating defensive reflexes such as coughing and respiratory depression in

bronchopulmonary C fibers[17,24,27]. In this context, TRPA1 expressed in the airway and lungs may detect O_2 toxicity at the frontline of defense against noxious chemical challenges.

Weather records[50] suggest that atmospheric PO_2 at sea level ranges between approximately 137 and 170 mm Hg. Because our O_2 dependence data reveal that minimal TRPA1 activity at 137 mm Hg is approximately 30% of the maximum at 170 mm Hg (**Fig. 3b**), so-called normoxia can be hyperoxic for mammalian TRPA1 channels, as reported in the context of O_2 avoidance in *Caenorhabditis elegans*[9] and insects[10].

METHODS

Electrochemical characterization of reactive disulfides. Half-wave potential ($E_{1/2}$) values of reactive disulfides and O_2 were determined by rotating disk-electrode voltammetry. The measurements were carried out with a BAS 100B (Bioanalytical Systems) and an RDE-3 rotating disk electrode (Nikko Keisoku) with an SC-5 controller (Nikko Keisoku). Reactive disulfides and O_2 were dissolved in dehydrated DMSO (Sigma). Reactive disulfides were then bubbled with argon gas through the solution. The voltammetry was measured in 0.1 M Bu_4NBF_4 in DMSO using a glassy carbon working electrode, a platinum wire counter electrode and an Ag/Ag^+ reference electrode at 2,500 r.p.m. $E_{1/2}$ is an empirical value that is defined as the midpoint of the rise of current in a voltammogram and, as such, it differs from the standard reduction potential ($E°$) of the compound. As previously reported[28], the relative nature of $E_{1/2}$ values presented in this study was deemed a relevant descriptor of the redox potential of these agents.

Cell cultures and cDNA expression. HEK 293 and HEK 293T cells were cultured similarly as previously described[14] and were co-transfected with recombinant plasmids and pEGFP-F (Clontech) as a transfection marker using SuperFect Transfection Reagent (Qiagen) and Lipofectamine 2000 (Invitrogen), respectively. $[Ca^{2+}]_i$ measurement, TIRF microscopy, DTNB-2Bio labeling assay and immunoprecipitation were performed 32–48 h after transfection[14]. Electrophysiological measurements were performed 32–72 h after transfection.

$[Ca^{2+}]_i$ measurements. $[Ca^{2+}]_i$ was measured as previously described[20]. Hyperoxic solution was achieved by bubbling with 22%, 24%, 26%, 28%, 30%, 32%, 34%, 36%, 80% or 100% O_2 (balanced with N_2) gas for at least 20 min before cell perfusion. Hypoxic solution was achieved by bubbling with 0%, 8%, 10%, 12%, 14%, 16% or 18% O_2 (balanced with N_2) gas at least 20 min before cell perfusion and by blowing the gas over the surface of the experimental chamber using a modified dish. The concentration of dissolved O_2 in the chamber solution was determined with an O_2 microelectrode (InLab 605, METTLER TOLEDO). A pH of 7.4 was maintained in the buffers after bubbling with N_2 gas, O_2 gas or both. Unless otherwise indicated, dissolved PO_2 measured in hypoxic, normoxic and hyperoxic solutions was 10% O_2, 20% O_2 and 86% O_2, respectively. More detailed description is described in **Supplementary Methods**.

Electrophysiology. Currents from cells were recorded at room temperature (22–25 °C) using patch-clamp techniques. Ramp pulses were applied every 5 s or 10 s from −100 mV to +100 mV or from +100 mV to −100 mV at a speed of 1.1 mV ms^{-1} from a V_h of 0 mV. For the conventional whole-cell recordings, the external solution contained 100 mM NaCl, 2 mM calcium gluconate and 10 mM HEPES (adjusted to pH 7.4 with NaOH, and osmolality adjusted to 320 mmol kg^{-1} with D-mannitol). The pipette solution contained 100 mM cesium aspartate, 5 mM BAPTA, 1.4 mM calcium gluconate, 2 mM disodium adenosine triphosphate, 2 mM $MgSO_4$, 1 mM $MgCl_2$, 10 mM HEPES and 10 mM $Na_5P_3O_{10}$ (pH 7.4 adjusted with CsOH, and osmolality adjusted to 320 mmol kg^{-1} with D-mannitol; 30 nM calculated free Ca^{2+}). For inside-out patch recordings, the external solution contained 50 mM cesium aspartate, 50 mM CsCl, 1 mM $MgCl_2$, 1 mM $CaCl_2$, 10 mM EGTA, 10 mM $Na_5P_3O_{10}$ and 10 mM HEPES (adjusted to pH 7.4 with cesium hydroxide, and osmolality adjusted to 300 mmol kg^{-1} with D-mannitol). The pipette solution contained 100 mM CsCl, 1 mM $MgCl_2$, 1 mM EGTA and 10 mM HEPES (adjusted to pH 7.4 with CsOH and osmolality adjusted to 300 mmol kg^{-1} with D-mannitol). A pH of 7.4 was maintained in the buffers after bubbling with N_2 gas, O_2 gas or both. Unless otherwise indicated, dissolved PO_2 measured in hypoxic, normoxic and hyperoxic solutions were 10% O_2, 20% O_2 and 86% O_2, respectively. More detailed description is provided in **Supplementary Methods**.

Peptide hydroxylation assay. The synthetic peptide PYGLKNLRPEFMQMQQIKEL, corresponding to $TRPA1_{386–405}$, at 40 μM was incubated with 2 μM of purified PHD2 in a final volume of 10 μl in buffer solution (adjusted to pH 7.4 with CsOH) containing 50 mM CsCl, 50 mM CsOH, 50 mM L-aspartic acid, 10 mM HEPES, 3 mM ascorbic acid, 0.1 mM $FeCl_2$, 0.3 mM 2-oxoglutarate, 1 mM DTT and 0.3 mg ml^{-1} catalase (Sigma) at 25 °C overnight. For MALDI-TOF mass spectrometric analyses, α-cyano-4-hydroxycinnamic acid solution was prepared in acetonitrile in water containing 0.1% trifluoroacetic acid (50:50 (v/v)) at a concentration of 10 mg ml^{-1}. Assay solution (1 μl) was mixed with α-cyano-4-hydroxycinnamic acid solution (5 μl) and spotted onto the target plate. Mass spectrometric analyses of the samples were performed with an Autoflex III (Bruker Daltonics).

Isolation of mouse nodose ganglion and DRG neurons. Nodose ganglion and DRG neurons were prepared from adult wild-type, *Trpa1* knockout, *Phd1* knockout and *Phd3* knockout mice as described previously[20]. The isolated cells were subjected to $[Ca^{2+}]_i$ and electrophysiological measurements 8–24 h after plating.

Recording of multifiber vagal afferent discharges. Mice were anesthetized with intraperitoneal injection of urethane, artificially ventilated through L-shaped tracheal cannula perforated at the corner and then paralyzed with 0.15 mg kg^{-1} panchronium bromide. To record vagal afferent activities, the distal cut end was placed on a pair of silver hook electrodes. Multifiber vagal nerve discharges were amplified (10,000× , AVB-8, Nihon Kohden), full-wave rectified, leaky integrated (time constant = 1 s, EI-601G, Nihon Kohden) and stored in a hard disk through an analog-to-digital converter (PowerLab, ADInstrument) together with original nerve discharges. Rectified and integrated vagal nerve activities were subtracted by noise level to obtain each nerve activity. Normoxic and hyperoxic gas challenges lasted 40 s and hypoxic challenge lasted 30 s. More detailed description is provided in **Supplementary Methods**.

Statistical analyses. All data are expressed as means ± s.e.m. We accumulated the data for each condition from at least three independent experiments. The statistical analyses were performed using the Student's *t*-test. P values < 0.05 were considered significant.

Additional methods. Further details on materials, cDNA cloning and plasmid construction, synthesis of AP-18, DTNB-2Bio labeling assay, expression and purification of recombinant PHD2, coimmunoprecipitation, TIRF microscopy, siRNA suppression, cell-surface labeling experiments, mice, RNA isolation and RT-PCR, immunohistochemistry, and semiquantitative RT-PCR analysis and recording of superior laryngeal discharges are in **Supplementary Methods**.

Received 8 May 2011; accepted 1 July 2011
published online 28 August 2011

References

1. Lane, N. *Oxygen: The Molecule That Made the World* (Oxford Univ. Press, Oxford, 2002).
2. Gonzalez, C., Almaraz, L., Obeso, A. & Rigual, R. Carotid body chemoreceptors: from natural stimuli to sensory discharges. *Physiol. Rev.* **74**, 829–898 (1994).
3. Neubauer, J.A. & Sunderram, J. Oxygen-sensing neurons in the central nervous system. *J. Appl. Physiol.* **96**, 367–374 (2004).
4. Weir, E.K., López-Barneo, J., Buckler, K.J. & Archer, S.L. Acute oxygen-sensing mechanisms. *N. Engl. J. Med.* **353**, 2042–2055 (2005).
5. Howe, A., Pack, R.J. & Wise, J.C. Arterial chemoreceptor-like activity in the abdominal vagus of the rat. *J. Physiol. (Lond.)* **320**, 309–318 (1981).
6. De Sanctis, G.T., Green, F.H. & Remmers, J.E. Ventilatory responses to hypoxia and hypercapnia in awake rats pretreated with capsaicin. *J. Appl. Physiol.* **70**, 1168–1174 (1991).
7. Gruss, M. *et al.* Moderate hypoxia influences excitability and blocks dendrotoxin sensitive K^+ currents in rat primary sensory neurones. *Mol. Pain* **2**, 12 (2006).
8. Longhurst, J.C. Tjen-A-Looi, S.C. & Fu, L.W. Cardiac sympathetic afferent activation provoked by myocardial ischemia and reperfusion. Mechanisms and reflexes. *Ann. NY Acad. Sci.* **940**, 74–95 (2001).
9. Gray, J.M. *et al.* Oxygen sensation and social feeding mediated by a *C. elegans* guanylate cyclase homologue. *Nature* **430**, 317–322 (2004).
10. Hetz, S.K. & Bradley, T.J. Insects breathe discontinuously to avoid oxygen toxicity. *Nature* **433**, 516–519 (2005).
11. Clapham, D.E. TRP channels as cellular sensors. *Nature* **426**, 517–524 (2003).
12. Voets, T., Talavera, K., Owsianik, G. & Nilius, B. Sensing with TRP channels. *Nat. Chem. Biol.* **1**, 85–92 (2005).
13. Hara, Y. *et al.* LTRPC2 Ca^{2+}-permeable channel activated by changes in redox status confers susceptibility to cell death. *Mol. Cell* **9**, 163–173 (2002).
14. Yoshida, T. *et al.* Nitric oxide activates TRP channels by cysteine S-nitrosylation. *Nat. Chem. Biol.* **2**, 596–607 (2006).
15. Xu, S.Z. *et al.* TRPC channel activation by extracellular thioredoxin. *Nature* **451**, 69–72 (2008).
16. Aarts, M. *et al.* A key role for TRPM7 channels in anoxic neuronal death. *Cell* **115**, 863–877 (2003).
17. Bessac, B.F. *et al.* TRPA1 is a major oxidant sensor in murine airway sensory neurons. *J. Clin. Invest.* **118**, 1899–1910 (2008).
18. Hinman, A., Chuang, H.H., Bautista, D.M. & Julius, D. TRP channel activation by reversible covalent modification. *Proc. Natl. Acad. Sci. USA* **103**, 19564–19568 (2006).

19. Macpherson, L.J. *et al.* Noxious compounds activate TRPA1 ion channels through covalent modification of cysteines. *Nature* **445**, 541–545 (2007).
20. Takahashi, N. *et al.* Molecular characterization of TRPA1 channel activation by cysteine-reactive inflammatory mediators. *Channels (Austin)* **2**, 287–298 (2008).
21. Story, G.M. *et al.* ANKTM1, a TRP-like channel expressed in nociceptive neurons, is activated by cold temperatures. *Cell* **112**, 819–829 (2003).
22. Nagatomo, K. & Kubo, Y. Caffeine activates mouse TRPA1 channels but suppresses human TRPA1 channels. *Proc. Natl. Acad. Sci. USA* **105**, 17373–17378 (2008).
23. Gracheva, E.O. *et al.* Molecular basis of infrared detection by snakes. *Nature* **464**, 1006–1011 (2010).
24. Bessac, B.F. & Jordt, S.E. Breathtaking TRP channels: TRPA1 and TRPV1 in airway chemosensation and reflex control. *Physiology (Bethesda)* **23**, 360–370 (2008).
25. Caterina, M.J. *et al.* The capsaicin receptor: a heat-activated ion channel in the pain pathway. *Nature* **389**, 816–824 (1997).
26. Nagata, K., Duggan, A., Kumar, G. & García-Añoveros, J. Nociceptor and hair cell transducer properties of TRPA1, a channel for pain and hearing. *J. Neurosci.* **25**, 4052–4061 (2005).
27. Nassenstein, C. *et al.* Expression and function of the ion channel TRPA1 in vagal afferent nerves innervating mouse lungs. *J. Physiol. (Lond.)* **586**, 1595–1604 (2008).
28. Topol, I.A. *et al.* Experimental determination and calculations of redox potential descriptors of compounds directed against retroviral zinc fingers: Implications for rational drug design. *Protein Sci.* **10**, 1434–1445 (2001).
29. Wallace, T.J., Schriesheim, A. & Bartok, W. The base-catalyzed oxidation of mercaptans. III. Role of the solvent and effect of mercaptan structure on the rate determining step. *J. Org. Chem.* **28**, 1311–1314 (1963).
30. Petrus, M. *et al.* A role of TRPA1 in mechanical hyperalgesia is revealed by pharmacological inhibition. *Mol. Pain* **3**, 40 (2007).
31. Kim, D. & Cavanaugh, E.J. Requirement of a soluble intracellular factor for activation of transient receptor potential A1 by pungent chemicals: role of inorganic polyphosphates. *J. Neurosci.* **27**, 6500–6509 (2007).
32. Schofield, C.J. & Ratcliffe, P.J. Oxygen sensing by HIF hydroxylases. *Nat. Rev. Mol. Cell Biol.* **5**, 343–354 (2004).
33. Webb, J.D., Coleman, M.L. & Pugh, C.W. Hypoxia, hypoxia-inducible factors (HIF), HIF hydroxylases and oxygen sensing. *Cell. Mol. Life Sci.* **66**, 3539–3554 (2009).
34. Bezzerides, V.J., Ramsey, I.S., Kotecha, S., Greka, A. & Clapham, D.E. Rapid vesicular translocation and insertion of TRP channels. *Nat. Cell Biol.* **6**, 709–720 (2004).
35. Schmidt, M., Dubin, A.E., Petrus, M.J., Earley, T.J. & Patapoutian, A. Nociceptive signals induce trafficking of TRPA1 to the plasma membrane. *Neuron* **64**, 498–509 (2009).
36. Bandell, M. *et al.* Noxious cold ion channel TRPA1 is activated by pungent compounds and bradykinin. *Neuron* **41**, 849–857 (2004).
37. Kwan, K.Y. *et al.* TRPA1 contributes to cold, mechanical, and chemical nociception but is not essential for hair-cell transduction. *Neuron* **50**, 277–289 (2006).
38. Aragonés, J. *et al.* Deficiency or inhibition of oxygen sensor Phd1 induces hypoxia tolerance by reprogramming basal metabolism. *Nat. Genet.* **40**, 170–180 (2008).
39. Bishop, T. *et al.* Abnormal sympathoadrenal development and systemic hypotension in PHD3−/− mice. *Mol. Cell. Biol.* **28**, 3386–3400 (2008).
40. Takeda, K. *et al.* Placental but not heart defects are associated with elevated hypoxia-inducible factor α levels in mice lacking prolyl hydroxylase domain protein 2. *Mol. Cell. Biol.* **26**, 8336–8346 (2006).
41. Dinkova-Kostova, A.T. *et al.* Direct evidence that sulfhydryl groups of Keap1 are the sensors regulating induction of phase 2 enzymes that protect against carcinogens and oxidants. *Proc. Natl. Acad. Sci. USA* **99**, 11908–11913 (2002).
42. Hathout, Y. *et al.* Characterization of intermediates in the oxidation of zinc fingers in human immunodeficiency virus type 1 nucleocapsid protein P7. *Drug Metab. Dispos.* **24**, 1395–1400 (1996).
43. Voss, A.A., Lango, J., Ernst-Russell, M., Morin, D. & Pessah, I.N. Identification of hyperreactive cysteines within ryanodine receptor type 1 by mass spectrometry. *J. Biol. Chem.* **279**, 34514–34520 (2004).
44. Ghezzi, P. Regulation of protein function by glutathionylation. *Free Radic. Res.* **39**, 573–580 (2005).
45. Hu, H., Bandell, M., Petrus, M.J., Zhu, M.X. & Patapoutian, A. Zinc activates damage-sensing TRPA1 ion channels. *Nat. Chem. Biol.* **5**, 183–190 (2009).
46. Wang, Y.Y., Chang, R.B. & Liman, E.R. TRPA1 is a component of the nociceptive response to CO_2. *J. Neurosci.* **30**, 12958–12963 (2010).
47. Semenza, G.L. & Wang, G.L. A nuclear factor induced by hypoxia via de novo protein synthesis binds to the human erythropoietin gene enhancer at a site required for transcriptional activation. *Mol. Cell. Biol.* **12**, 5447–5454 (1992).
48. Meller, S.T. & Gebhart, G.F. A critical review of the afferent pathways and the potential chemical mediators involved in cardiac pain. *Neuroscience* **48**, 501–524 (1992).
49. Kubin, L., Alheid, G.F., Zuperku, E.J. & McCrimmon, D.R. Central pathways of pulmonary and lower airway vagal afferents. *J. Appl. Physiol.* **101**, 618–627 (2006).
50. Mcelroy, M.B. *The Atmospheric Environment: Effects of Human Activity* (Princeton University Press, 2002).

Acknowledgments

We thank D. Julius, T. Yoshida and M. Wakamori for experimental advice, T. Miki and J. Ikenouchi for helpful discussions, and T. Morii and I. Hamachi for their support in DTNB-2Bio synthesis. We are also grateful to T. Niidome, H. Shirakawa and T. Nakagawa for their support in mouse experiments.

Author contributions

N.T., S. Kiyonaka, Y. Mizuno and Y. Mori initiated and designed the project. N.T., S. Kiyonaka, T. Numata, D.K., Y. Mizuno, S.Y., S.N., T.O., S. Kaneko and T. Nokami performed experiments and analyzed data. T.K. supervised *in vivo* studies. S.S. and J.Y. supervised the electrochemical experiments. E.K. and P.C. established *Phd1* knockout and *Phd3* knockout mouse lines subjected to the experiment. N.T., T.K., S. Kiyonaka, T. Numata, D.K. and Y. Mori wrote the manuscript. Y. Mori directed the research. All authors discussed and commented on the manuscript.

Competing financial interests

The authors declare no competing financial interests.

Additional information

Supplementary information is available online at http://www.nature.com/naturechemicalbiology/. Reprints and permissions information is available online at http://www.nature.com/reprints/index.html. Correspondence and requests for materials should be addressed to Y. Mori.